Segmentation of the F2 Leading Edge in a Backscatter Sounder Ionogram

Rafal Sienicki, Manuel A. Cervera, Philip H. W. Leong

***Abstract*—Backscatter sounder systems co-located with Over-the-Horizon Radar (OTHR) can be leveraged to provide a near real-time characterisation of the ionospheric propagation conditions to aid the OTHR surveillance mission. Ionogram inversion can be performed using features derived from a backscatter ionogram to infer the optimum OTHR operational parameters and to enable the geolocation of the detected targets. In this paper, we demonstrate the application of a deep learning segmentation model on a backscatter ionogram dataset obtained from the Jindalee Operational Radar Network (JORN) frequency management system to extract the F2 leading edge feature. Our results show that deep learning is a viable method for leading edge feature identification and extraction in backscatter ionogram imagery.**

***Index Terms*—Ionogram scaling, ionosphere, segmentation, Over-the-Horizon Radar.**

I. Introduction

THE ionosphere is a region of the Earth's atmosphere that contains free electrons and is able to refract High Frequency (HF)[1] (3-30 MHz) radio waves. An OTHR exploits this feature to provide a long range, beyond line-of-sight surveillance capability. The ionosphere is a highly dynamic medium that varies temporally and spatially over many different scales, hence characterisation of the ionosphere is crucial for the effective operation of an OTHR.

Ionospheric sounder equipment is used to measure and quantify the properties of the ionosphere by the transmission and reception of HF radio waves. Vertical Incidence Sounder (VIS) and Oblique Incidence Sounder (OIS) systems are commonly used for this purpose. A VIS measures the ionospheric properties directly above it (the transmitter and receiver are co-located), whilst an OIS measures the ionospheric properties at the mid-point between a transmitter and receiver separated by several hundred or thousands of kilometers. A key challenge for the use of VIS and OIS systems to support OTHR operation is to ensure the sounder measurement footprints overlap with OTHR coverage requirements. However, physical, practical and legal constraints on sounder transmitter and receiver placement may render the sounder network sub-optimal for OTHR application. In this situation, a Backscatter Sounder (BSS) is more suitable for the OTHR use-case. The quasi co-location of receiver and transmitter systems and similar two-way propagation mode of the BSS and OTHR systems makes the BSS attractive for OTHR application [1] [2].

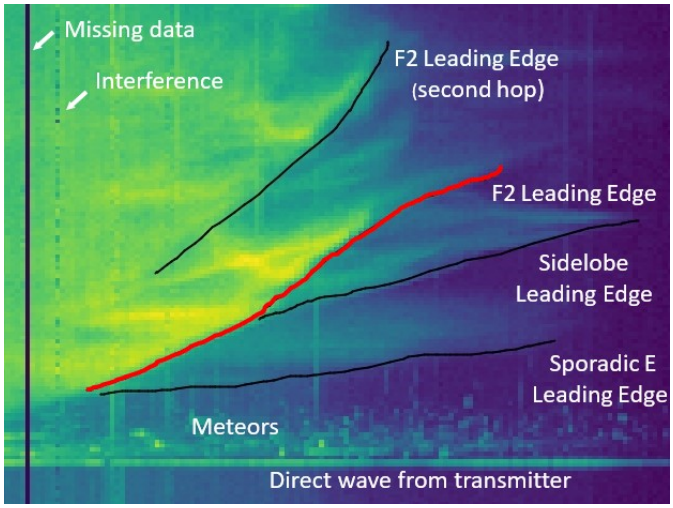

Fig. 1: Cropped sample backscatter sounder ionogram image showing labelled dominant features. The image represents return signal strength as a function of group range (vertical axis) and radio wave frequency (horizontal axis). The F2 leading edge (red line) is used as a target for the supervised segmentation training presented in this research. Returns from meteors, interference signals and missing data pixels are also shown.

The return signal strength recorded by ionospheric sounders, when displayed as a function of group range[2] vs radio wave frequency, is known as an ionogram. An example of a BSS ionogram is presented in Figure 1. These ionograms are evaluated to identify critical features and parameters that subsequently can be used to estimate the electron density vertical profile. This process is known as ionogram scaling[3]. Sienicki et al. [3] reviews ionogram features and scaling techniques for different ionospheric sounders. Traditionally, ionogram scaling has been performed by ionospheric subject matter experts; however, manual scaling is a time intensive and laborious activity and hence numerous automatic scaling

Manuscript received mm dd, YYYY; revised MM DD, YYYY.

[1]Ionospheric effects on radio wave propagation are not exclusive to this band i.e. propagation effects occur at frequencies both below and above the HF band limits.

[2]Time-of-flight of the radio wave multiplied by the speed of light in vacuo.

[3]In this paper, the term 'scaling' is used in reference to all ionograms recorded by VIS, OIS and BSS sounders. The authors acknowledge that the term does not have the same meaning for BSS and VIS/OIS ionogram categories. In the latter case, scaling refers to feature identification and parameterisation of ionospheric properties. This is the conventional interpretation of the term in the ionospheric research community. In the former case, the term refers to a more limited capability. Here, scaling refers to the identification of features from which information regarding propagation modes may be inferred, without any subsequent ionospheric parameterisation.

techniques have been investigated and developed over the last few decades. The vast majority of automated scaling algorithms have been applied to VIS ionograms, and to a lesser extent, OIS ionograms, with limited attention to BSS ionograms [3]. The scaling of BSS ionograms is more challenging and the least mature. The integration of returns from multiple propagation modes and antenna sidelobes, the variable ground backscatter, and the reduced number of non-ambiguous visually discernible image features increases the scaling complexity.

The Leading Edge (LE) is the primary feature of interest of a BSS ionogram. A LE is a thin, ledge-like feature that is visually discernible as a series of connected, steep signal strength (pixel intensity) changes. It is the minimum time delay (group range) for the receipt of the backscattered, ionospherically propagated signal as a function of frequency [4]. Typically, the LE trace exhibits a smooth, low-order polynomial-like profile with the contour line trending upwards as a function of frequency. Each group range coordinate on the LE trace corresponds to a unique ground range for the backscattered ray(s) with respect to frequency.

Multiple LE traces, corresponding to propagation via different propagation modes, are commonly observed on a BSS ionogram. Key LE features are labelled in the backscatter ionogram depicted in Figure 1. The LE trace associated with returns from the F2 ionospheric layer, referred to as F2LE, is the most important BSS ionogram feature that is critical for ionogram inversion. The F2LE is labelled as a red trace in Figure 1.

In this work, we train a deep learning segmentation model, the U-Net [5] model, on a labelled JORN BSS ionogram dataset to demonstrate an automated F2LE feature extraction functionality. The main contributions of our research include:

1) The proposal of a novel loss function based on Focal and Negative Log Likelihood loss terms. As will be shown, this is optimised for BSS ionogram F2LE accuracy and leads to improved results over simpler approaches.
2) A new set of metrics customised for BSS ionogram LE feature extraction. In particular, we propose accuracy and recall metrics defined in terms of the scaled frequency error with respect to a surveillance region of interest.
3) Application of deep learning techniques to F2LE segmentation which achieves a 94% accuracy and 93% recall. To the best of our knowledge, this is the first time deep learning has been applied to F2LE segmentation.

II. Related Works

Ionogram scaling features are visually discernible as a series of curved, connected trace segments representing a pattern of signal strength variation that is governed by ionospheric propagation conditions. Visual discernment of the critical features in ionograms is complicated by noise, interference, sounder equipment failures, returns from "unusual" ionospheric layers (e.g. sporadic E layer) and ionospheric disturbances. The effects of these phenomena can be observed on an ionogram as distortion, smearing, blurring and masking of important ionogram features. Consequently ionogram scaling is a challenging task, particularly for ionograms captured in disturbed ionospheric conditions.

A significant amount of research has been conducted into automatic scaling for VIS and OIS ionograms over the last few decades. Techniques such as data fitting [6]–[8], template matching [9], [10], computer vision [11], [12], Kalman filtering [13], fuzzy logic [14] and more recently, machine learning [10], [11], [15] have been investigated for automatic scaling. This research has produced a number of automatic scaling tools. POLAN [7], ARTIST [6], Autoscala [16] and DST-IIP [10] are example scaling tools that have been demonstrated to reliably extract features in VIS ionograms. For the OIS case, there is a reduced number of scaling tools; however, details of several algorithms have been published [10], [11], [15], [17]. Sienicki et al. [3] provides an up-to-date comprehensive review of the automatic scaling techniques and tools.

The BSS is significantly larger, more complex and expensive than the VIS and OIS, hence it is not as common and there is no publically available BSS dataset. Consequently, the scaling of BSS ionograms is the least mature.

Identification and extraction of LE features in a BSS ionogram is a challenging undertaking. Firstly, the LE is a ledge-like feature with undefined start or end points. It does not resemble visually discernible features such as cusps, asymptotic lines or vertices that are present in VIS and OIS ionograms. Secondly, the effects of ionospheric dynamics and sounder characteristics can profoundly influence the LE feature. Consequently, the LE may exhibit intensity variation that can render some aspects of the trace line to be faint, disconnected, or exhibit localised strong curvature features, e.g. kinks. Thirdly, discrimination logic is required to separate the LE traces based on refractions from different ionospheric layers (including multiple hops). This is complicated by apparent LE features associated with azimuthal sidelobes of the receive array beamformer.

There are very few publications covering investigations for BSS ionogram scaling with no authoritative scaling tools matching the pedigree of VIS scaling tools such as ARTIST. Techniques based on the Kalman filter [18], minimum group path theory [19], [20], polynomial line fitting [19] and image processing [21] are the main approaches investigated. [19] is the sole reference that includes experimental results, albeit for a small dataset recorded by a low power BSS.

In this work, we apply a deep learning model on a dataset recorded by a high power BSS system. Higher power increases the signal-to-noise ratio, which reveals more ionospheric features within the ionograms. This can reveal complications such as contributions from the receive array sidelobes, which may be problematic for automated scaling algorithms.

III. Dataset

Data collected from two BSS sub-systems of the Royal Australian Air Force (RAAF) JORN Frequency Management System (FMS) [1] are used in this study. Each sounder performs measurements for 8 azimuthal beams spanning a bandwidth of 5-45 MHz, with a 200 kHz and 50 km frequency and range resolution respectively [1]. The measurement data

originates from the year 2014 spanning a range of diurnal and seasonal conditions.

A total of 779 ionogram images from the JORN FMS dataset are used as a basis for this investigation. The first hop F2LEs were manually labelled by DST Group senior and junior ionospheric specialists to enable supervised segmentation model training. The trace label is a continuous line with arbitrary start and end points. An example of a labelled BSS ionogram is presented in Figure 1. For this study, only the F2LE label is used (red line) as a target signal.

The ionogram images were formatted into a 697x924 pixel image size, converted into greyscale format and normalised. The x-y coordinates of the F2LE label were used to generate a pixel level, binary mask.

IV. Method

We treat the F2LE identification and extraction task as a supervised segmentation challenge. In this work, we apply a deep learning Fully Connected Convolutional (FCN) encoder-decoder U-Net architecture that has achieved success in the biomedical field [5].

In many deep learning image segmentation investigations it is common to use the distribution based Binary Cross Entropy (BCE) and/or region based soft Dice Loss (DL) functions for model training [22]. These loss functions demonstrate good performance for segmentation of natural and medical targets. However, one drawback for this type of loss function design is that the shape or contour of the target is not taken into consideration. It has been found that such a loss function design is not suitable for application to images that contain ambiguous or discontinuous boundaries [23].

To address this limitation, we use a distance map to capture the shape and geometrical profile of the thin, one-dimensional BSS ionogram F2LE feature. A distance map is a matrix, with the same dimensions as the original input image, that stores the values of the Euclidean distance of each pixel to the closest point on the target mask, defined in the two-dimensional image coordinate space. The distance map is queried to determine distance information for each pixel of interest during loss calculations. Figure 2 shows a sample of a F2LE distance map mask that is used for model training in this investigation. The generation of distance map is a computationally expensive task; however, this task only needs to be performed once, and can be performed offline.

We apply a Negative Log Likelihood (NLL) function to enable the U-Net model to learn the segmentation of the F2LE feature. The pixel-wise distance map is used to derive mean and standard deviation parameters of the Normal distribution. This function is used to guide the model to produce a segmentation output that is as close as possible to the F2LE label. The equation of the NLL function is defined in Equation 1:

$$\mathcal{L}_{NLL} = -log\frac{1}{\sigma\sqrt{2\pi}}e^{-\frac{1}{2}\left(\frac{-\mu}{\sigma}\right)^2} \tag{1}$$

where μ and σ are respectively the mean and standard devation of the pixel-wise distance distribution of a segmentation prediction. The NLL function acts to impose a higher loss penalty

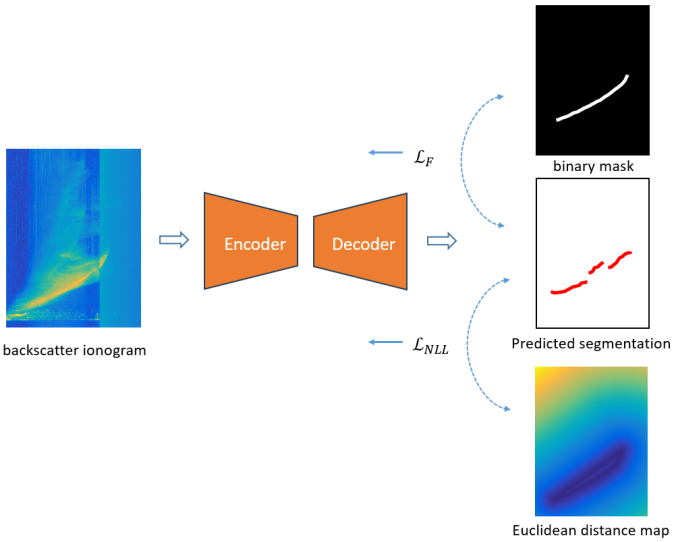

Fig. 2: In this investigation, a U-Net encoder-decoder model is used to segment the F2LE feature. The model accepts a backscatter ionogram as input. A binary mask derived from manual labels is used to compute the focal loss component. A Euclidean distance map (based on the binary mask) is used to derive a pixel-wise NLL distribution loss component.

for predictions that are distant from the labelled F2LE trace. This is in contrast to the DL function, a popular segmentation loss function, that solely takes into account the degree-of-overlap without consideration of pixel distance.

To account for the highly imbalanced nature of our dataset, we integrate a Focal Loss (FL) term into our loss function, a variant of the BCE function that is designed for application in highly imbalanced datasets [24]. A lower loss term is imposed on background pixels to enable increased focus on rare, foreground pixels. The FL function is defined in Equation 2:

$$\mathcal{L}_F = -1\,(1-p_t)^{\gamma}\,log\,(p_t) \tag{2}$$

where p_t is the estimated pixel probability and γ is a tunable focussing parameter.

The loss function for the F2LE segmentation model is composed of focal and NLL terms as follows:

$$\mathcal{L} = \mathcal{L}_F + \mathcal{L}_{NLL} \tag{3}$$

An architecture diagram of our design is presented in Figure 2.

V. Experimentation and Metrics

We apply a 10-fold cross validation scheme with a 90% train-test split on the dataset to ensure our model does not overfit on the relatively small dataset.

Table I outlines the main model hyper-parameters that were used in our experimentation. These parameters were derived using a manual grid search approach.

Parameter	Value
batch size	4
number of epochs	200
learning rate	1e-4 reduced to 1e-7, using a cosine annealing learning rate scheduler
Focal loss focussing parameter γ	2
mask threshold	0.5

TABLE I: Model hyper-parameters used in this investigation.

Unlike the VIS[4] ionogram case for which a scaling standard exists [25] and is used in many automatic VIS scaling tools to report scaling performance, no equivalent standard exists for the BSS ionogram scaling application. An obvious metric is based on the pixel-wise distance between the estimated and truth (manually labelled) LE traces. Given that a BSS ionogram LE trace exhibits an undefined length with no fixed start or end coordinates, a decision needs to be made on how many, and which LE pixels should be used as reference pixels for metric calculations.

In this work, we use a BSS ionogram scaling domain specific metric to evaluate segmentation performance. The scaling error is reported in the ionogram frequency domain[5] in terms of accuracy and recall scores. These scores are calculated for a sample OTHR surveillance region. Inspired by [26], in this investigation we report a frequency scaling error referenced to a surveillance region spanning a group-range interval of 1200-2800km[6] and evaluated at 400km intervals. These evaluation group range lines are marked as dotted horizontal lines in the sample ionogram segmentation results shown in Figure 3.

Accuracy is defined as the mean pixel-wise distance between the estimated and truth LE pixels, defined in the frequency dimension. This is reported as a frequency scaling error. Instead of reporting the absolute error, as is done by Crouch [26], we report the scaling error as a ratio of results that are within an acceptable margin of error. This approach provides a more meaningful interpretation of segmentation accuracy to the OTHR operator. In this investigation, we set the acceptable error margin to 1 MHz.

The recall metric, also reported as a ratio, quantifies the relative number of segmentation results reported by a segmentation model, and can be used to infer the number of missed (False Negatives) F2LE detections. In this investigation, a missed F2LE detection is reported for the case when no F2LE pixels are returned by the segmentation model for a reference group range.

For both accuracy and recall metric calculations, a mean score is reported. This reflects the average performance based on the five reference group range pixels in each ionogram, evaluated on the test dataset. To ensure a consistent and repeatable evaluation, all five reference pixel coordinates[7] in each test ionogram are used to calculate the metric scores. This is in contrast to [19], where scaling results are reported in terms of the number of instances where a minimum number (three out of five) of estimated LE pixels are within an error margin.

[4]Whilst no such standard exists for the OIS case, the similary of features in OIS and VIS ionograms, deems it acceptable for the same standard to be applied to the OIS ionogram case.

[5]Evaluation of scaling error in the frequency domain, as opposed to the group range, is more useful for the OTHR application.

[6]This group range region represents a portion of the F2LE trace that exists in the majority of the ionograms considered in the dataset used for this investigation.

VI. Results and Discussion

Table II details the results from our experiments conducted on the JORN BSS dataset. A U-Net segmentation model configured with a loss function composed of NLL and FL terms achieves the best result (shown in bold). This model performs pixel-wise segmentation of the F2LE feature with an accuracy corresponding to an upper-bound 1MHz scaling error for 94% of test cases with a 93% recall rate.

U-Net Loss function	Accuracy (Frequency Scaling Error) (% results with $\leq$ 1 MHz)	Recall (%)
wBCE	90.6	89.9
wBCE + DL	92.0	61.3
FL	92.6	92.1
wBCE + NLL	93.0	89.1
FP + NLL	**94.1**	**92.6**

TABLE II: F2LE segmentation experiment results. *wBCE = weighted Binary Cross Entropy, DL = Dice Loss, NLL = Negative Log Likelihood, FL = Focal Loss.*

Inspection of the segmented F2LE trace generated for the BSS ionogram test dataset reveals that in the majority of cases the LE trace is segmented correctly. The segmented LE pixels are consistent with the human labelled F2LE trace. The first (top) image presented in Figure 3 represents a good F2LE segmentation result. In this ionogram, the segmented F2LE trace overlaps closely with the labelled F2LE trace, including group range evaluation pixels (identified as horizontal dotted lines). The second ionogram in Figure 3 also produces acceptable segmentation results referenced to the evaluation pixels; however, the performance is slightly reduced relative to the top ionogram, and certain aspects of the LE trace are disconnected.

Analysis of the results indicates that for some cases, aspects of the F2LE trace are incorrectly segmented. Many of these False Positive errors correspond to instances where the model identifies a leading edge of non-F2 ionospheric layers, higher order F2 hops or sidelobe returns as an F2LE pixel. The bottom ionogram in Figure 3 is an example where a portion of the sidelobe leading edges are falsely segmented as an F2LE. It is expected that training the model on a larger dataset will improve the model's ability to segment and discriminate LE pixels correctly for ionograms captured in wider set of ionospheric conditions.

The results also confirm that the segmentation performance is robust to ionogram interference and missing data artefacts.

Table II also includes results from our experimentation for different loss functions, including cross-entropy and dice loss

[7]For ionograms that did not include a LE pixel for the referenced group range evaluation line, a reduced number of evaluation LE pixels was used.

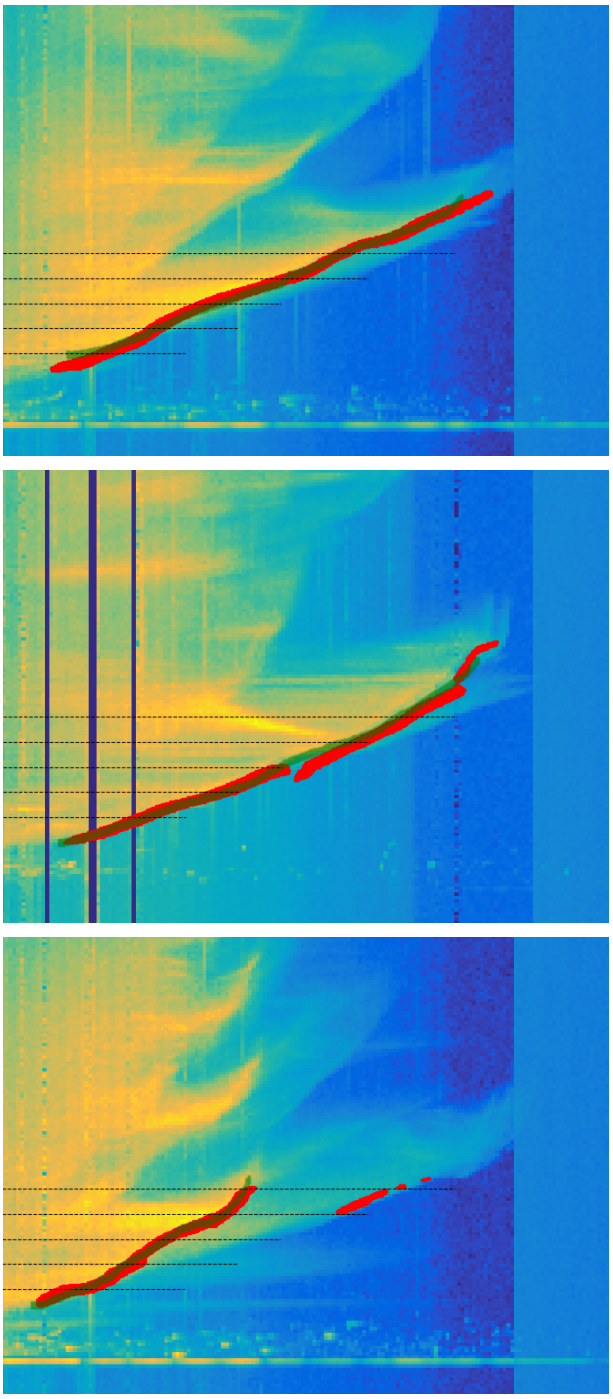

Fig. 3: Sample cropped BSS ionogram from the test dataset showing results from our deep learning segmentation model. Green trace = human labelled F2LE trace. Red trace = U-Net model F2LE segmentation output. Dotted horizonal lines = five reference group range lines used to quantify F2LE frequency scaling error. *Top image:* This represents a good segmentation result. The majority of extracted F2LE trace lies close to the truth F2LE trace. *Middle image:* Good segmentation results returned for all group range line evaluation pixels; however, some aspects of the F2LE trace are disconnected. *Bottom image:* Good segmentation result for the F2LE trace; however, some aspects of the sidelobe leading edge are also (falsely) classified as F2LE.

functions that are commonly applied for image segmentation. The results show that NLL and FL functions enhance the U-Net segmentation model's accuracy and recall performance respectively. An approximate 3% performance improvement is observed relative to results obtained from the cross entropy loss function. Fusion of these loss terms in a loss function (FP + NLL) serves to further improve the model's performance across both metrics.

Results shown in Table II also confirm that the DL function is not suited for the BSS ionogram LE segmentation application. In contrast to the performance improvement observed for the use of the DL function, when applied to object segmentation [27], we observe a performance degradation for the BSS ionogram dataset. The recall performance is reduced significantly when the loss function includes a DL component. This result indicates that an IoU based loss function may not be suitable for segmentation of a BSS ionogram LE feature.

VII. Conclusion

In this paper, we have applied the U-Net image segmentation model to the backscatter sounder data from the JORN. To the best of our knowledge, this is the first application of a deep learning segmentation model to a backscatter ionogram dataset. Experimental results show that our approach has been successful in extracting the F2LE feature in backscatter ionogram images.

This model can be extended to perform feature extraction of leading edges corresponding to E, Es (sporadic E), F1, higher order hops and sidelobe returns.

Future work will consider a larger dataset and integration of radio wave propagation theory and ionospheric physics with deep learning to produce a physics guided deep learning backscatter ionogram scaling model.

Acknowledgments

This work would not have been possible without access to a labelled ionogram dataset. We thank Danielle Edwards for the time taken to perform the laborious task of labelling hundreds of backscatter ionogram images.

We thank Lenard Pederick, Chris Crouch, David Netherway and Barry Flower for useful discussions and suggestions to support this research investigation.

References

[1] G. F. Earl and B. D. Ward, "The frequency management system of the Jindalee over-the-horizon backscatter HF radar," *Radio Science*, vol. 22, no. 2, pp. 275–291, 1987. [Online]. Available: https://agupubs.onlinelibrary.wiley.com/doi/abs/10.1029/RS022i002p00275,eprint=https://agupubs.onlinelibrary.wiley.com/doi/pdf/10.1029/RS022i002p00275

[2] S. V. Fridman, "Reconstruction of a three-dimensional ionosphere from backscatter and vertical ionograms measured by over-the-horizon radar," *Radio Science*, vol. 33, no. 4, pp. 1159–1171, 1998. [Online]. Available: https://agupubs.onlinelibrary.wiley.com/doi/abs/10.1029/98RS00477

[3] R. Sienicki, D. Edwards, M. A. Cervera, and P. Leong, "Ionogram scaling for vertical, oblique and backscatter sounders: a review of challenges and opportunities," 2025, manuscript submitted for publication.

[4] T. A. Croft, "Sky-wave backscatter: A means for observing our environment at great distances," *Reviews of Geophysics*, vol. 10, no. 1, pp. 73–155, 1972. [Online]. Available: https://doi.org/10.1029/RG010i001p00073

[5] O. Ronneberger, P. Fischer, and T. Brox, "U-Net: Convolutional Networks for Biomedical Image Segmentation," pp. 234–241, 10 2015.
[6] B. W. Reinisch and H. Xueqin, "Automatic calculation of electron density profiles from digital ionograms: 3. Processing of bottomside ionograms," *Radio Science*, vol. 18, no. 3, pp. 477–492, 1983. [Online]. Available: https://doi.org/10.1029/RS018i003p00477
[7] J. E. Titheridge, "Ionogram analysis with the generalised program POLAN," 1985. [Online]. Available: https://repository.library.noaa.gov/view/noaa/1343
[8] M. W. Fox and C. Blundell, "Automatic scaling of digital ionograms," *Radio Science*, vol. 24, no. 6, pp. 747–761, 1989. [Online]. Available: https://doi.org/10.1029/RS024i006p00747
[9] C. Jiang, G. Yang, Z. Zhao, Y. Zhang, P. Zhu, and H. Sun, "An automatic scaling technique for obtaining F2 parameters and F1 critical frequency from vertical incidence ionograms," *Radio Science*, vol. 48, no. 6, pp. 739–751, 2013. [Online]. Available: https://agupubs.onlinelibrary.wiley.com/doi/abs/10.1002/2013RS005223,eprint=https://agupubs.onlinelibrary.wiley.com/doi/pdf/10.1002/2013RS005223
[10] A. J. Heitmann and R. S. Gardiner-Garden, "A Robust Feature Extraction and Parameterized Fitting Algorithm for Bottom-Side Oblique and Vertical Incidence Ionograms," *Radio Science*, vol. 54, no. 1, pp. 115–134, 2019. [Online]. Available: https://doi.org/10.1029/2018RS006682
[11] N. J. Redding, "Image understanding of oblique ionograms: the autoscaling problem," in *1996 Australian New Zealand Conference on Intelligent Information Systems. Proceedings. ANZIIS 96*, 1996, Conference Proceedings, pp. 155–160.
[12] Z. Chen, S. Wang, S. Zhang, G. Fang, and J. Wang, "Automatic scaling of F layer from ionograms," *Radio Science*, vol. 48, no. 3, pp. 334–343, 2013. [Online]. Available: https://doi.org/10.1002/rds.20038
[13] F. Su, Z. Zhao, S. Li, M. Yao, G. Chen, and Y. Zhou, "Signal Identification and Trace Extraction for the Vertical Ionogram," *IEEE Geoscience and Remote Sensing Letters*, vol. 9, no. 6, pp. 1031–1035, 2012.
[14] L.-C. Tsai and F. T. Berkey, "Ionogram analysis using fuzzy segmentation and connectedness techniques," *Radio Science*, vol. 35, no. 5, pp. 1173–1186, 2000. [Online]. Available: https://agupubs.onlinelibrary.wiley.com/doi/abs/10.1029/1999RS002170,eprint=https://agupubs.onlinelibrary.wiley.com/doi/pdf/10.1029/1999RS002170
[15] A. Ippolito, D. Altadill, C. Scotto, and E. Blanch, "Oblique Ionograms Automatic Scaling Algorithm OIASA application to the ionograms recorded by Ebro observatory ionosonde," *J. Space Weather Space Clim.*, vol. 8, 2018. [Online]. Available: https://doi.org/10.1051/swsc/2017042
[16] C. Scotto, "A method for processing ionograms based on correlation technique," *Physics and Chemistry of the Earth, Part C: Solar, Terrestrial and Planetary Science*, vol. 26, no. 5, pp. 367–371, 2001. [Online]. Available: https://www.sciencedirect.com/science/article/pii/S1464191701000150
[17] Y. Hu, H. Song, X. Zou, and Z. Zhao, "Real-time automatic scaling method of oblique ionogram parameters based on morphological operator and inversion technique," *Wuhan University Journal of Natural Sciences*, vol. 20, no. 4, pp. 323–328, 2015. [Online]. Available: https://doi.org/10.1007/s11859-015-1100-2
[18] S. T. Hutchinson, "Scaling backscatter 1F leading edges," Internal Report, DST Group, 1994.
[19] H. Song, Y. Hu, C. Jiang, C. Zhou, and Z. Zhao, "Automatic scaling of HF swept-frequency backscatter ionograms," *Radio Science*, vol. 50, no. 5, pp. 381–392, 2015. [Online]. Available: https://doi.org/10.1002/2014RS005621
[20] M. S. Penzin, S. N. Ponomarchuk, V. P. Grozov, and V. I. Kurkin, "Real-Time Techniques for Interpretation of Ionospheric Backscatter Sounding Data," *Radio Science*, vol. 54, no. 5, pp. 480–491, 2019. [Online]. Available: https://doi.org/10.1029/2018RS006656
[21] M. McDonnell, "Wavelet based detection and fitting of backscatter ionogram leading edges," 2014.
[22] J. Ma, J. Chen, M. Ng, R. Huang, Y. Li, C. Li, X. Yang, and A. Martel, "Loss odyssey in medical image segmentation," *Medical Image Analysis*, vol. 71, p. 102035, 2021.
[23] F. Caliva, C. Iriondo, A. Morales Martinez, S. Majumdar, and V. Pedoia, *Distance Map Loss Penalty Term for Semantic Segmentation*, 2019.
[24] T. Y. Lin, P. Goyal, R. Girshick, K. He, and P. Dollár, "Focal loss for dense object detection," in *2017 IEEE International Conference on Computer Vision (ICCV)*, 2017, Conference Proceedings, pp. 2999–3007.
[25] W. R. Piggott and K. Rawer, "U.R.S.I. handbook of ionogram interpretation and reduction," 1978, (Karl). [Online]. Available: https://repository.library.noaa.gov/view/noaa/10404
[26] C. Crouch, "Using neural networks and deep learning to improve ionospheric model accuracy using high-frequency radar backscatter observations," Masters Research Thesis, University of Adelaide, 2018.
[27] F. Milletari, N. Navab, and S.-A. Ahmadi, "V-net: Fully convolutional neural networks for volumetric medical image segmentation," in *2016 fourth international conference on 3D vision (3DV)*. IEEE, 2016, Conference Proceedings, pp. 565–571.